

Refining the Experimental Extraction of the Number of Independent Samples in a Mode-Stirred Reverberation Chamber

Khalid Oubaha,¹ Martin Richter,¹ Ulrich Kuhl,¹ Fabrice Mortessagne,¹ and Olivier Legrand¹

¹*Institut de Physique de Nice, Université Côte d'Azur, CNRS, 06100 Nice, France*

(Dated: May 16, 2018)

We investigate the number of independent samples in a chaotic reverberation chamber. Its evaluation as defined by the IEC standard can be made more precise when using not the index of the first value larger than the correlation length but using the value obtained by a linear interpolation instead. The results are validated by a juxtaposition with values from a measurement using a high stirrer-angle resolution. A comparison with estimates known from the literature validates our findings. An alternative approach using the local maxima of the parametric dependence of the transmission is presented in order to show the applicability of the extracted correlation length over a large range of frequencies.

I. INTRODUCTION

Mode-stirred reverberation chambers play an important role in electromagnetic compatibility. With their help it is possible to obtain statistically valuable results for the electromagnetic radiation emitted from the object under test. However, in order to get reliable statements about the fluctuations of the EM field it is necessary to use statistically independent experimental realizations. In other words, the statistical ensemble usually achieved by a so-called mode stirrer has to be mixing enough to make the intensity patterns of the chamber statistically independent from each other. As the solution to Maxwell's equations under the given boundary conditions depend continuously on the latter, a sufficiently large change has to be performed. For mode stirrers, this usually means that the angle of rotation has to be sufficiently large, assuming the stirrer is not too small. Once this minimally necessary step width is determined the number of independent samples (NIS) from a full turn of the stirrer can be calculated [1]. This number is the main focus of this paper. Note that the results are obtained for an empty chamber. We do not expect that loading effects of typical devices under test will have a qualitative impact on our findings in a chaotic reverberation chamber (CRC).

Because of being such an important quantity there exist also rough estimates following geometrical arguments [2]. They are based on probabilistic estimates for rays of the EM field hitting the stirrer. Besides these predictions, one can use experimental data to extract the NIS. As the measured data is available only for a discrete set of stirrer positions the minimally necessary step width is technically only defined for these discrete values. As a consequence the NIS can fluctuate quite strongly with frequency. This can be overcome by either increasing the resolution of the stirrer movement or by interpolating the results. In this paper we will compare this interpolation for measurements performed in a chaotic reverberation chamber.

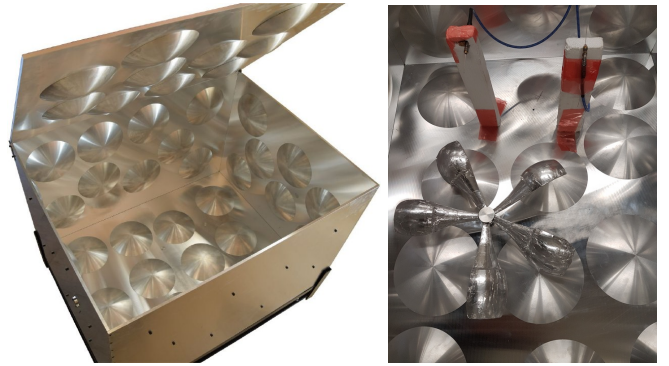


FIG. 1. Photograph of the chaotic reverberation chamber with length $L = 100$ cm, width $W = 77$ cm and height $H = 62$ cm. At the walls 54 spherical caps of radius $r_c = 10$ cm are used, 51 having a cap height of $h_c = 3$ cm and 3 having $h_c = 8$ cm. The total internal volume is $V = 0.44$ m³ (left). At the bottom a stirrer with 5 paddles is placed which can be turned by a stepper motor and acts as mode stirrer. The two monopole antennas were mounted on polystyrene blocks having a perpendicular polarization direction (right).

II. EXPERIMENTAL SETUP

The experiments were carried out in our chaotic reverberation chamber shown in Fig. 1. The Vector Network Analyzer (VNA, Rohde&Schwarz ZVA67) was attached to two monopole antennas inside the chamber (see Fig. 1(right)). For a total range of frequencies f from 0.5 GHz to 5.0 GHz we measured the complex transmission amplitude between the two antennas. The measurement was repeated for $N_\theta = 3600$ stirrer positions using a step of $\Delta\theta = 0.1^\circ$, Eq. (3). This range was chosen to cover frequencies from around the Lowest-Usable Frequency f_{LUF} [1, 3, 4] up to approximately $7 \cdot f_{LUF}$. Using the frequency of the 60th mode as a definition, the f_{LUF} of our homemade chaotic chamber is approximately 0.735 GHz.

Corresponding transmissions for three different frequency ranges with different values of the modal overlap

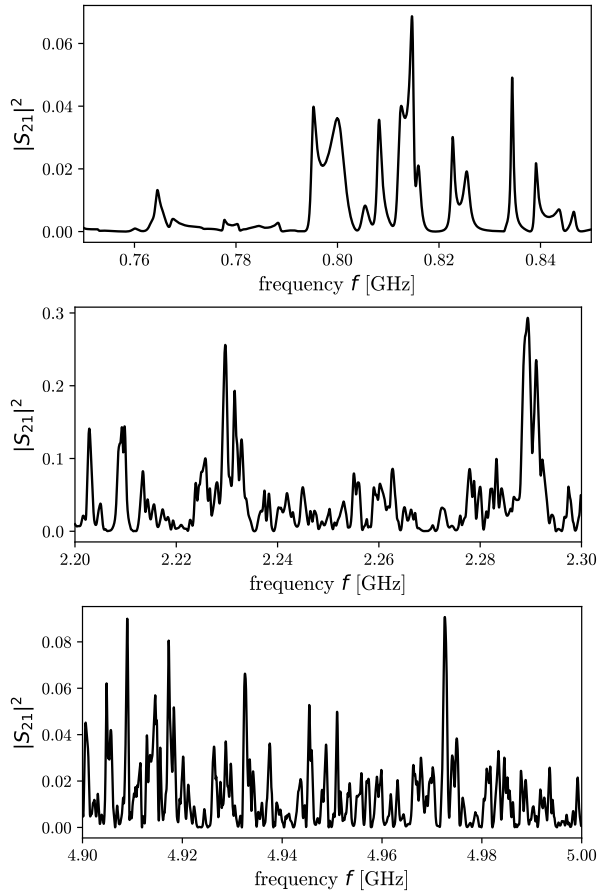


FIG. 2. Dependency of the transmission $|S_{21}|^2$ on frequency f for one fixed stirrer position $\theta = 1^\circ$. Three frequency ranges, representing different regimes of the modal overlap d , are shown: The lowest frequency range (top, $d = 0.3$), the highest frequency range (bottom, $d = 4.5$), and a frequency range in between corresponding to the example in Fig. 3 (middle, $d = 1.4$). For the values of d see Tab. I. The frequency range was chosen to cover 100 MHz in all plots.

for one fixed stirrer position versus frequency are shown in Fig. 2.

Besides the whole frequency range 0.5 – 5 GHz we focused on seven sub-intervals, where we measured with a higher frequency resolution to guarantee a proper extraction of the transmission maxima. The ranges have been chosen such that important parameters (see Tab. I) are sufficiently well defined. One important parameter is the mean frequency spacing of adjacent eigenmodes of the cavity, Δ_f , which we calculate using Weyl’s law, $\Delta_f = c^3/(8\pi V f^2)$. The signal decay time τ is determined from the exponential decay of the square modulus of the Fourier transform of the transmission [5],

$$I(t) = |\text{FT}(S_{21})(t)|^2 = I_0 e^{-t/\tau}, \quad (1)$$

where the transform is performed either over the frequency range of the seven sub-intervals or a frequency window of 100 MHz. The average quality factor Q is thus

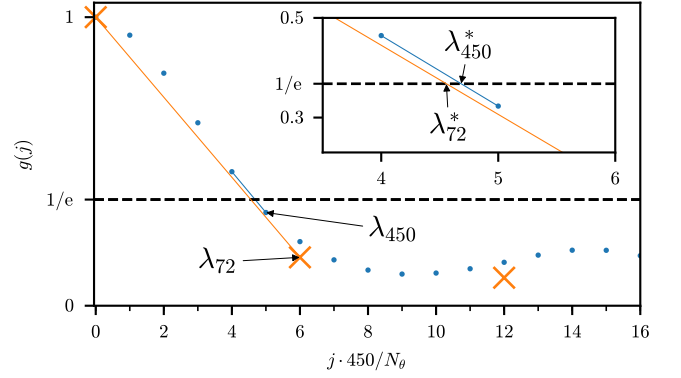


FIG. 3. Linear interpolation used to obtain the improved correlation length λ_θ^* (8) from the traditional value λ_θ (5). The plot is done for $f = 2.21$ GHz and therefore corresponds to the middle image of Fig. 2. Shown is the extraction for $N_\theta = 450$ (blue points) and $N_\theta = 72$ (orange crosses).

given by $Q = 2\pi\tau\langle f \rangle$, where $\langle f \rangle$ is the average frequency of the window used to calculate τ . Finally, the modal overlap d is obtained by

$$d = \frac{\text{mean decay rate}}{\text{mean eigenmode spacing}} = \frac{1/2\pi\tau}{\Delta_f} = \frac{\langle f \rangle}{Q\Delta_f}. \quad (2)$$

The extracted values can be found in Tab. I for the seven sub-intervals.

TABLE I. Figures of merit for the reverberation chamber at different frequencies ranges ($f_{\min} - f_{\max}$). Shown are the values for the mean frequency spacing Δ_f , the signal decay time τ , the mean distance between adjacent maxima δf_{\max} , the quality factor Q , and the modal overlap d . The frequency ranges are also indicated in Fig. 4.

$f_{\min} - f_{\max}$ Ghz	Δ_f kHz	τ ns	$\langle \delta f_{\max} \rangle$ kHz	Q 10^3	d
0.75 – 0.85	3734.43	203	1422.05	0.8	0.3
1.1 – 1.25	1731.13	180	1603.75	1.0	0.7
1.7 – 1.85	758.59	203	1422.05	2.0	1.2
2.2 – 2.40	451.80	276	1045.92	3.7	1.4
2.8 – 2.90	294.25	343	841.62	5.9	1.6
3.8 – 4.0	157.14	345	836.74	8.4	3.0
4.9 – 5.0	97.54	361	799.65	11.2	4.5

III. REFINING THE EXTRACTION OF THE NUMBER OF INDEPENDENT SAMPLES

The usual approach to extract the NIS is to use the autocorrelation function of the transmission data. Given N_θ equidistant angles at which the transmission ampli-

tude $S_{21}(f_i, \theta_j)$ has been measured,

$$\theta_j = (j-1) \cdot \Delta\theta, \quad \Delta\theta = \frac{360^\circ}{N_\theta}, \quad j = 1, \dots, N_\theta, \quad (3)$$

we can calculate for a given frequency f , see Refs. [1, 6, 7]

$$g_f(j) = \frac{1}{N_\theta - 1} \frac{\sum_{k=1}^{N_\theta} x(f, \theta_k) x(f, \theta_{k+j})}{\sum_{k=1}^{N_\theta} x(f, \theta_k)^2} \quad (4)$$

where $x = \tilde{x} - \langle \tilde{x}(f) \rangle$, $\langle \tilde{x}(f) \rangle = \frac{1}{N_\theta} \sum_{j=1}^{N_\theta} \tilde{x}(f, \theta_j)$, and $\tilde{x} = |S_{21}|^2$ and we use that S_{21} is periodic in θ . In Fig. 3 an example from our measured data is shown for $N_\theta = 450$ (blue points) and $N_\theta = 72$ (orange crosses). For simplicity we only use one stirrer although generalizations to multiple stirrers exist [8].

Assuming an exponential decay of correlations, $g_f(j) \sim e^{-j/\lambda(f)}$, one defines the correlation length λ_θ as the smallest integer for which

$$g_f(\lambda_\theta(f)) \leq e^{-1} \approx 0.37. \quad (5)$$

In case of small sample size the definition has to be refined by using (see Eq. (A.5) in Ref. [1])

$$g_f(\lambda_\theta(f)) \leq 0.37 \left(1 - \frac{7.22}{N_\theta^{0.64}} \right). \quad (6)$$

Note that Eq. (5) was given in the IEC standard version of 2003. The refinement Eq. (6) was suggested in the version of 2011. While this alters the determined NIS, the change is not of qualitative nature as can be seen from the comparison of Eq. (5) and Eq. (6) in Fig. 4. The main difference is seen as expected for small values like $N_\theta = 72$ which, for the older norm saturates at its maximum value $N = 72$ for large frequencies. For the current norm this saturation is not reached. In Fig. 4 (lower) we apply the current norm also for $N_\theta = 72$ although it is strictly speaking just valid for $N_\theta \geq 100$. A detailed analysis of the literature on which the norm is based [9] reveals that there is no apparent reason for not using the norm for $N_\theta = 72$. In the following we use the older norm, Eq. (5), as it makes the comparison for different sample sizes N_θ easier to understand. The λ_θ are indicated by λ_{450} and λ_{72} in Fig. 3. This value is usually used in the literature to define the number of independent field components as [1, 2]

$$N(f) = \frac{N_\theta}{\lambda_\theta(f)}. \quad (7)$$

If the correlation decays quickly, then the extracted value of $\lambda_\theta(f)$ fluctuates between small integer values when changing the frequency. Therefore, N might express large fluctuations. These would vanish if a smaller $\Delta\theta$ would be used as this would result in a higher resolution of λ_θ according to Eq. (5), see Fig. 5 for example.

A refined method can be obtained by linearly interpolating the two points before and after the critical value (5)

is undercut,

$$\lambda_\theta^* = \lambda_\theta - \frac{\frac{1}{e} - g(\lambda_\theta)}{g(\lambda_\theta - 1) - g(\lambda_\theta)} \quad (8)$$

$$N^*(f) = \frac{N_\theta}{\lambda_\theta^*(f)}. \quad (9)$$

This approach is justified by the fact that a larger N_θ and therefore higher angle resolution (3) yields a finer resolution of the autocorrelation function. In the inset of Fig. 3 the values obtained by using this fit for two different N_θ are shown. The resulting values are quite close, whereas using the index directly would lead to large differences in N . In our experiment we checked this assumption by comparing the data with a reduced data set like in Ref. [7], see Sec. II. Note that due to the fact that $\lambda_\theta - 1 < \lambda_\theta^* \leq \lambda_\theta$, the extracted NIS fulfills $N^* \geq N$. Furthermore, using the decay of the autocorrelation function only estimates the number of uncorrelated samples. However, this approach has become normative for the determination of the NIS in the literature.

A. Number of Independent Samples

We calculated the number of independent samples (7) based on the integer-valued correlation length (5) and the interpolated value (9) based on Eq. (8), respectively. The analysis was done once for the whole frequency range 0.5 – 5 GHz. We determine the independent samples using either the whole set of measured angles ($N_\theta = 3600$, $\Delta\theta = 0.1^\circ$) or two reduced data sets [7] with $N_\theta = 450$ ($\Delta\theta = 0.8^\circ$) and $N_\theta = 72$ ($\Delta\theta = 5^\circ$). The value of $N_\theta = 450$ is commonly used in the literature as suggested in the standard [1] but not without criticism [6, 7, 10].

In order to check whether the linear interpolation of formula (8) works for our experimental data, it is shown in Fig. 3 for $f = 2.21$ GHz using the $N_\theta = 450$ (shown as blue dots) and for a strongly reduced number of $N_\theta = 72$ (shown as large crosses). On the one hand one can see that the values λ_{450} and λ_{72} obtained using the discrete numbers deviate, whereas the values of λ_{450}^* and λ_{72}^* are quite close (after an appropriate rescaling). In this example one can also see that the interpolation is justified as the decay of the correlation around $1/e$ is approximately linear. Have in mind that Fig. 3 is using a rescaled value of the integer $j \cdot 450/N_\theta$ due to the reduction of angles, so that the axis corresponds to the index j in the case $N_\theta = 450$. Note that the interpolation also works close to f_{LUF} as our reverberation chamber is rendered fully chaotic due to the spherical caps at the walls [3].

The overall dependency of the NIS versus the full frequency range for different calculation methods is shown in Fig. 4. Because one observes large fluctuations with frequency, we applied a rectangular frequency filter. In general, such large fluctuations make the extraction of the NIS by using only a single frequency questionable. For increasing frequencies the averaged NIS rises as the

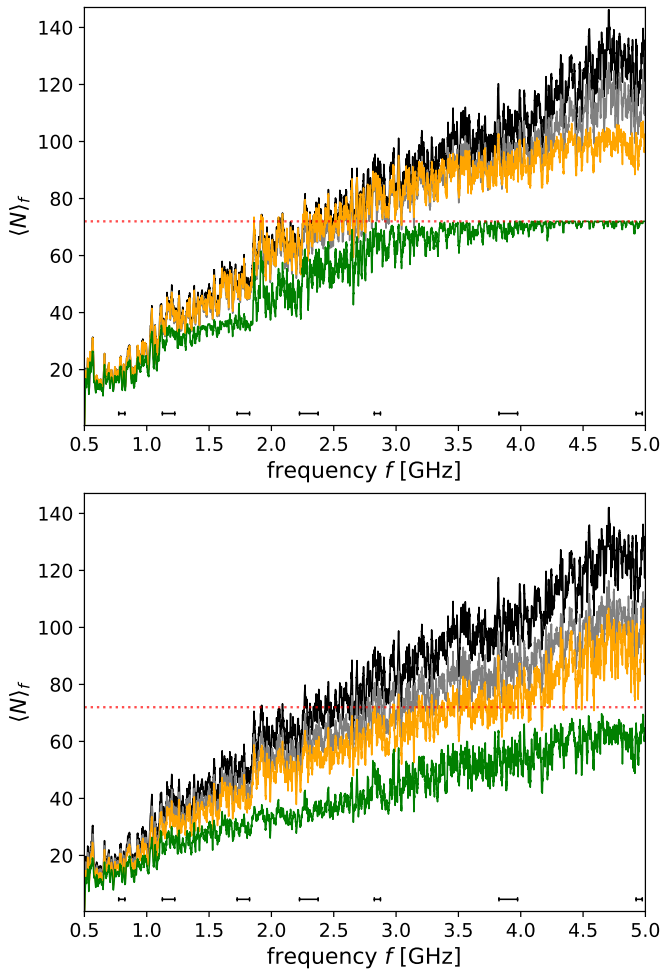


FIG. 4. Number of independent samples for frequency range 0.5 – 5 GHz determined by the minimal integer (7) and by the linear interpolation (9) (upper) as well as the curves given by Eq. (7) based on a correlation length from Eq. (6) (lower). The different curves belong to the different angle resolutions, namely $N_\theta = 3600$ (black), $N_\theta = 450$ (gray), $N_\theta = 72$ (green). For $N_\theta = 72$ the values obtained by linear interpolation (9) are also shown (orange). The black intervals at the bottom indicate the ranges used in Tab. I. The red dotted line indicates $N = 72$. All curves show frequency-smoothed values after applying a rectangular-filter of 100 frequency steps (10 MHz).

stirrer position is better resolved by the EM field in accordance with the estimates from Ref. [2]. This higher resolution of the stirred volume increases the sensitivity with respect to the stirrer position and thereby decreases the correlation length. The data using the 3600 (black curve) and 450 (orange curve) samples are following each other closely apart from small deviation at higher frequencies. In case of 72 samples the NIS is bounded at $N = N_\theta$ (red dotted line). In this case, λ_θ is always 1 as the first corresponding value of g_f in Eq. (5) already lies below the threshold, $g_f(1) \leq 1/e$ (see also Fig. 3). Additionally we plotted the curve for 72 samples where we used the linear interpolation to obtain λ_{72}^* to calculate the NIS

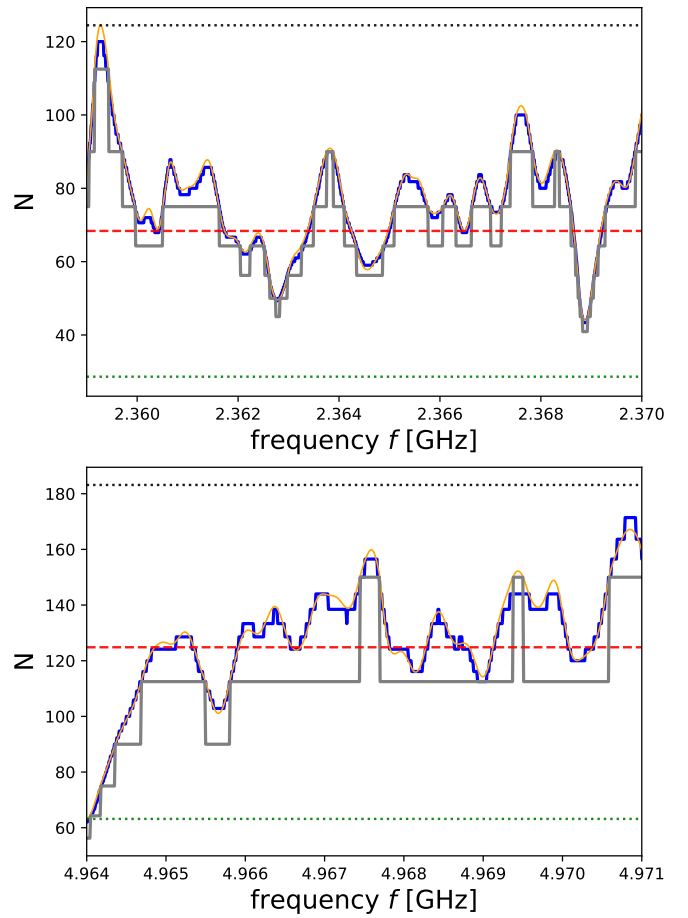


FIG. 5. Number of independent samples for two small frequency ranges. Shown is a zoom of the data from two subsets of Tab. I (2.2 – 2.4 GHz top, 4.9 – 5 GHz bottom). We compare the standard approach Eq. (7) for $N_\theta = 450$ (gray) and $N_\theta = 3600$ (blue) with N^* obtained for $N_\theta = 450$ (orange) via the interpolation Eq. (9). The maximum and minimum values (black and green dotted lines) as well as the average (red dashed line) of the interpolation for $N_\theta = 450$ (orange curve) over the whole corresponding frequency range of the corresponding sub-window (see Tab. I) are added for comparison. In contrast to Fig. 4, no frequency average is applied.

(see Fig. 4, orange curve). This curve follows better the curves with larger N_θ and even gives values above 72. While technically the 72 sample cannot have more than 72 independent data sets, the linear interpolation outlines a possibility to estimate which angular resolution is a good choice for getting as many independent samples with a minimal amount of measurements.

Indicated in the figure are also the seven frequency sub-ranges, for which parameters are detailed in Tab. I. Fig. 5 shows $N(f)$ and $N^*(f)$ for two of these frequency subsets as well as for different stirrer resolutions N_θ . Here, no frequency average was applied. Note that the smaller sample size leads to larger step sizes in the frequency axis in case of the calculation via Eq. (7). On the one hand side we find that the larger $N_\theta = 3600$ is always above

the smaller $N_\theta = 450$ value but the value obtained by the linear interpolation for $N_\theta = 450$ follows nicely the $N_\theta = 3600$ case.

B. Prediction of the Number of Independent Samples

The above extracted values for the number of independent samples can be compared with an estimate based on the volume V and quality factor Q of the chamber [2]. The prediction is based on a probabilistic argument that the stirred volume V_{stirrer} is hit by a beam in the chamber. It differs for large and small stirrers, N_1 and N_s , respectively. In our case the volume affected by the stirrer as defined in Ref. [2] is

$$V_{\text{stirrer}} = 0.0034 \text{ m}^3. \quad (10)$$

For the low frequency range the estimate is given by [2]

$$N_s = C_s \frac{\lambda V_{\text{stirrer}}^{2/3}}{V} Q, \quad V_{\text{stirrer}} \ll \lambda^3 \quad (11)$$

whereas in the high frequency range it should be related to

$$N_1 = C_1 \frac{V_{\text{stirrer}}}{V} Q, \quad V_{\text{stirrer}} \gg \lambda^3. \quad (12)$$

When both expressions are adjusted to the experimental data in the appropriate frequency range we obtain $C_s = 1.55$ and $C_1 = 1.56$, respectively. In Fig. 6 the averaged number of independent samples is compared to the two predictions. A good agreement is found to (11) (red circles) in the small frequency range ($V_{\text{stirrer}}^{1/3}/\lambda < 0.5$, see upper axis) and to (12) (blue triangles) in the high frequency range ($V_{\text{stirrer}}^{1/3}/\lambda > 1.75$, see upper axis). Also the values of C_s and C_1 are of the order of one agreeing with values obtained in [2]. In view of the two curves we propose here an interpolating estimate with two fitted prefactors which are compatible with the extracted values over the full frequency range. This formula reads

$$N^{\text{interpol}}(f) = \left(C_1 + C_s \frac{c/f}{V_{\text{stirrer}}^{1/3}} \right) \frac{V_{\text{stirrer}}}{V} Q(f) \quad (13)$$

where we use the frequency dependent values of the Q factor $Q = 2\pi\tau\langle f \rangle$ to fit Eq. (13) against the data. The fit using only small and large frequency values yields $C_s = 1.87$, $C_1 = 0.7$. The resulting dark blue curve is shown in Fig. 6. The estimate (13) follows reasonably well over the whole frequency range.

C. Velocities of Local Maxima

We can extract the local maxima f_{max} [5] from the measured transmission in the seven sub-intervals mentioned in Tab. I. In order to get reliable results we

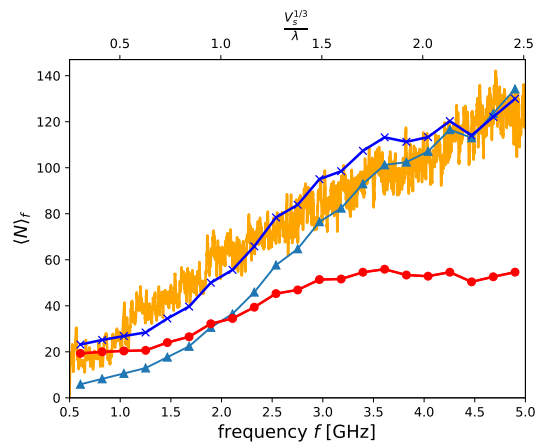


FIG. 6. Comparison of the number of independent samples with the estimate based on geometrical arguments. Based on the experimental data for $N_\theta = 3600$ we fit the prefactor in Eq. (11) (red circles) and Eq. (12) (light blue triangles). The interpolating formula (13) matches the whole frequency range (dark blue curve). The corresponding values are $C_s = 1.87$, $C_1 = 0.7$. The experimental curve shows frequency-smoothed values after applying a rectangular-filter of 100 frequency steps (10 MHz).

smoothed the $|S_{21}(f, \theta)|^2$ along the frequency axis using a Hann filter of window size 100 for all data sets. We then extracted the local maxima of the intensity for each value of the stirrer position. In the following we want to demonstrate that the statistical properties of the maxima are similar to one another across the frequency ranges shown, once the appropriate scaling has been applied. If the resonances are isolated (i.e., the modal overlap d is small ($d \ll 1$)) the local maxima are defined by the frequencies of the eigenmodes ν_n . The dependence of the eigenvalues on a parameter p have been studied extensively in the framework of “Quantum Chaos” [11, 12] for scalar fields, but can be directly applied to the vectorial problem. Defining a level velocity $v_n = d\nu_n/dp$ one can distinguish global and local perturbation. In case of a global perturbation in a CRC the distribution of the level velocities v_n is Gaussian [13], whereas for local perturbations it shows a Bessel K distribution [14]. This would be another possibility to characterize the quality of the stirring. In case of a chaotic system the levels show avoided crossing, whereas in case of regular, more precisely, integrable systems, the levels will cross [11, 12]. The frequency scale of importance is the mean frequency spacing Δ_f . In Fig. 7(top) the dynamics of the local maxima is presented for the low frequency range, which has $d = 0.3$, thus showing reasonably isolated resonance. The spectra should be uncorrelated when the local maxima go from one avoided crossing to another, which agrees visually with the calculated correlation length λ_θ indicated by the horizontal arrow. Studies also exist in the case of open systems [15] on eigenmode dynamics, but in the case of moderate or large modal overlap, the fre-

quencies of the eigenmodes are not directly related to the local maxima we extracted here. To define the frequency scale in case of strong modal overlap we need to estimate the mean spacing between transmission maxima, which has been obtained by Schroeder and Kuttruff [16], $\delta f_{\max} = 1/(2\sqrt{3}\tau)$, an expression which is assumed to be valid for $d > 3$. If abscissa and ordinate are scaled appropriately the behavior of the ridges of maxima $f_{\max}(\theta)$ is similar with respect to the distances of close encounters and the steepness with respect to the stirrer angle, i.e., $\frac{df_{\max}}{d\theta}$. Using the correlation length λ_θ for each of these frequency ranges as read from, e.g., Fig. 5, we can choose the scale of the abscissa of these plots to cover several correlation lengths. We chose the θ range from $\theta_{\min} = 100^\circ$ to $\theta_{\max} = \theta_{\min} + 3 \cdot \langle \lambda_\theta^*(f) \rangle_f \cdot \Delta\theta$ to cover 3 times the correlation length in each figure. The ordinate was scaled using the values from Tab. I in the following way: For frequency ranges with a modal overlap smaller than $d \leq 1$ we chose a plot range of width $8 \cdot \Delta f$. For the other ranges we used the estimate δf_{\max} and chose $8 \cdot \delta f_{\max}$. The corresponding plots are shown in Fig. 7 for three of the seven intervals from Tab. I. Each of the plots contains two arrows indicating the correlation length λ_θ and the mean spacing between maxima, respectively. Due to the scaling of the abscissa the one for λ_θ has the same length in every plot.

We can indeed see a qualitative agreement between the average distance between the extracted f_{\max} ridges, thus confirming the results obtained in the previous chapter.

IV. CONCLUSION

This paper presents experimental data from a mode-stirred chaotic reverberation chamber and estimates the number of independent samples (NIS) for a 360° turn of the stirrer. We compare the reduced data set for $N_\theta = 450$ steps usually found in the literature with a finer ($N_\theta = 3600$) and coarser subdivision ($N_\theta = 72$) of the full angle. The corresponding values of the NIS extracted by the usual procedure (7) show a very coarse dependency if N_θ is reduced. We compare this value with an improved estimate based on a linear interpolation (8) of the correlation length. The values obtained in this way for the coarser measurements resemble very much the full data set as shown, for example, in Fig. 5. We compare these numbers also with predictions (11), (12) from Ref. [2] and find quantitative agreement if we use the interpolation formula (13), see Fig. 6. We check that the results are valid for conceptually different regimes, i.e. frequency ranges for which the modal overlap d of the chamber is smaller, around, or larger than 1, see Tab. I.

To emphasize the findings with an independent approach, we focus on the extraction of local maxima of the transmission [5]. The detailed resolution of $N_\theta = 3600$ allows to follow $f_{\max}(\theta)$ as the stirrer moves. The cor-

responding dynamics show fluctuations on a scale which is expected to be similar to the correlation length λ_θ .

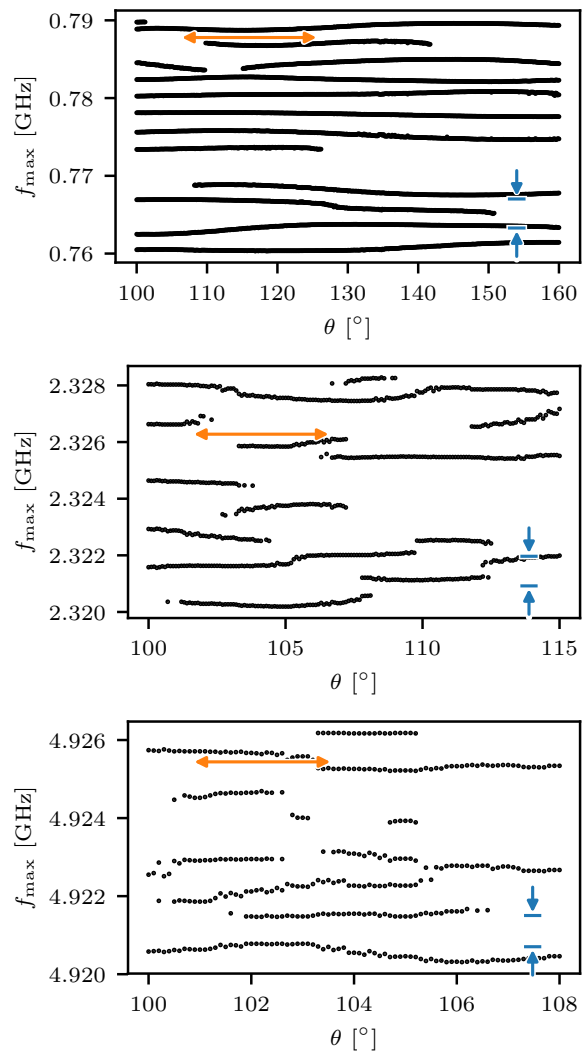


FIG. 7. Dependency of the local maxima f_{\max} on stirrer position θ . Depicted are three of the seven frequency ranges from Tab. I. The horizontal arrow indicates the correlation length λ_θ . The vertical arrows indicate Δf (upper figure) or δf_{\max} (middle and lower figure). The abscissa are scaled to cover $3 \cdot \lambda_\theta$. The ordinates are scaled to cover $8 \cdot \Delta f$ (upper figure) or $8 \cdot \delta f_{\max}$ (middle and lower figure).

Hence, we show that scaling a plot of f_{\max} using λ_θ yields qualitatively the same image.

ACKNOWLEDGMENT

We would like to thank the European Commission for financial support through the H2020 programme by the Open Future Emerging Technology ‘‘NEMF21’’ Project (664828).

-
- [1] “Electromagnetic compatibility (EMC) - part 4-21: Testing and measurement techniques - reverberation chamber test methods,” (2011), ser. Blue Book, No. 4, International Electrotechnical Commission (IEC) International Standard IEC 61 000-4-21:2011, 2011. [Online]. Available: <https://webstore.iec.ch/publication/4191>.
- [2] Paul Hallbjörner, “A model for the number of independent samples in reverberation chambers,” *Microwave and Optical Technology Letters* **33**, 25–28 (2002).
- [3] J.-B. Gros, U. Kuhl, O. Legrand, F. Mortessagne, O. Picon, and E. Richalot, “Statistics of the electromagnetic response of a chaotic reverberation chamber,” *Adv. Electromagn.* **4**, 38 (2015).
- [4] J.-B. Gros, U. Kuhl, O. Legrand, and F. Mortessagne, “Lossy chaotic electromagnetic reverberation chambers: Universal statistical behavior of the vectorial field,” *Phys. Rev. E* **93**, 032108 (2016).
- [5] U. Kuhl, O. Legrand, F. Mortessagne, K. Oubaha, and M. Richter, “Statistics of reflection and transmission in the strong overlap regime of fully chaotic reverberation chambers,” in *2017 47th European Microwave Conference (EuMC, Nuremberg)* (2017) arXiv:1706.04873, Presented at the European Microwave Week in Nuremberg 2017.
- [6] O. Lundén and M. Bäckström, “Stirrer efficiency in FOA reverberation chambers. Evaluation of correlation coefficients and chi-squared tests,” in *IEEE International Symposium on Electromagnetic Compatibility. Symposium Record (Cat. No.00CH37016)*, Vol. 1 (2000) pp. 11–16.
- [7] H. G. Krauthäuser, T. Winzerling, J. Nitsch, N. Eulig, and A. Enders, “Statistical interpretation of autocorrelation coefficients for fields in mode-stirred chambers,” in *2005 International Symposium on Electromagnetic Compatibility, 2005. EMC 2005.*, Vol. 2 (2005) pp. 550–555.
- [8] G. Gradoni, V. Mariani Primiani, and F. Moglie, “Reverberation chamber as a multivariate process: FDTD evaluation of correlation matrix and independent positions,” *Prog. Electromagn. Res.* **133**, 217–234 (2013).
- [9] H.G. Krauthäuser, “Grundlagen und Anwendungen von Modenverwirbelungskammern,” (2007), Habilitationsschrift, Otto-von-Guericke-Universität Magdeburg, ISBN: 978-3-929757-43-9.
- [10] C. Lemoine, P. Besnier, and M. Drissi, “Advanced method for estimating number of independent samples available with stirrer in reverberation chamber,” *Electronics Letters* **43**, 861–862 (2007).
- [11] F. Haake, *Quantum Signatures of Chaos. 2nd edition* (Springer, Berlin, 2001).
- [12] H.-J. Stöckmann, *Quantum Chaos - An Introduction* (University Press, Cambridge, 1999).
- [13] B. D. Simons and B. L. Altshuler, “Universal velocity correlations in disordered and chaotic systems,” *Phys. Rev. Lett.* **70**, 4063 (1993).
- [14] M. Barth, U. Kuhl, and H.-J. Stöckmann, “Global versus local billiard level dynamics: The limits of universality,” *Phys. Rev. Lett.* **82**, 2026 (1999).
- [15] E. N. Bulgakov, I. Rotter, and A. F. Sadreev, “Phase rigidity and avoided level crossings in the complex energy plane,” *Phys. Rev. E* **74**, 056204 (2006).
- [16] M. R. Schroeder and K. H. Kuttruff, “On frequency response curves in rooms. comparison of experimental, theoretical, and monte carlo results for the average frequency spacing between maxima,” *J. Acoust. Soc. Am.* **34**, 76 (1962).